第 26 卷 第 4 期
2004 年 7 月

岩 土 工 程 学 报
Chinese Journal of Geotechnical Engineering

Vol. 26 No. 4
July, 2004

A constitutive model for evaluating small to large cyclic strains of saturated sand during liquefaction process
评价饱和砂土液化过程中小应变到大应变的本构模型

ZHANG Jiarmin(张建民), WANG Gang(王 刚)
(Institute of Geotechnical Engineering, Department of Hydraulic Engineering, Tsinghua University, Beijing 100084, China)

Abstract: A new simplified effective stress constitutive model is presented for evaluating small to large cyclic strains of saturated sand during liquefaction process. It is developed by refining and modifying Ramberg-Osgood model in the following three aspects: ①A formulation for asymptotic movements of both MPTL(Moving Phase Transformation Line) and MCSL(Moving Critical State Line) is incorporated to accurately describe the effective stress path and the critical stress state; ②A stress degradation model is used to describe the stress-dilatancy and to define the degradation and hardening of the skeleton curve with variation of excess pore water pressure; ③A new post-liquefaction deformation theory is incorporated to model large shear strain response in cyclic undrained loading after initial liquefaction. The results calculated by the proposed model have been compared favorably with experimental observations. The new model is suitable for dynamic response analysis of level or nearly level saturated sand ground.

Key words: sand; constitutive relationship; large shear strain; post-liquefaction; Ramberg-Osgood Model
CLC number: TU 435 **Document code**: A **Article ID**: 1000- 4548(2004)04- 0546- 07

Biography: ZHANG Jiarmin(1960-), Male, PhD, Professor.

摘 要: 在 Ramberg-Osgood 模型的基础上,建立了一个实用的能描述饱和砂土从液化前小应变到初始液化后大应变范围的非线性本构模型。该模型主要有三个特点: ①采用作者曾提出的移动相态转换线(MPTL)和移动临界状态线(MCSL)概念来较为合理地描述变形过程中的有效应力路径和临界状态; ②采用一个应力软化模型来描述剪胀和定义超静孔压变化引起的骨架曲线的软化与硬化; ③基于笔者等提出的液化后大变形理论来描述初始液化后产生的大剪切变形。文中通过对室内循环剪切试验结果的模拟,验证了模型的预测能力。该模型适用于水平饱和砂土地基的有效应力地震反应分析。

关键词: 砂土; 本构模型; 液化后大变形; Ramberg- Osgood 模型

0 Introduction*

Realistic modeling of boundary-value problems of soil dynamics requires a detailed knowledge of dynamic stress - strain behavior of soil. Several cyclic constitutive soil models have been developed from extensive experimental and theoretical researches. They may be classified into two main categories, i. e. plastic models and nonlinear elastic models. The cyclic plastic models published already mainly include: ①multi-surface models; ②bounding surface models or two-surface models; and ③multi-mechanisms models. These cyclic plastic models can be used to simulate basic contractive and dilative trends of soil under simple cyclic loadings, and reproduce cyclic effective stress path and related deformation in some limited loading conditions. Unfortunately, none of these models can provide a satisfactory prediction of cyclic mobility for loose to dense sand over a wide range from small to large strains. Accurate prediction using these models is obtained only in limited conditions, by introducing both considerable complexity and idealized material assumptions. In addition, the evaluation of the model parameters is another very difficult problem in practice.

Pragmatic dynamic effective stress analysis using nonlinear elastic models has been developed in the past decades. The nonlinear models mainly include Ramberg-Osgood model and its modifications[1~4] as well as hyperbolic model and its modifications[5~8]. When a nonlinear model is used in the earthquake response analysis of saturated sand deposits the following important factors must be considered[8]: ① The initial shear modulus in situ; ② the variation of shear modulus with shear strain; ③ contemporaneous generation and dissipation of pore water pressure; ④changes in mean effective stress; ⑤damping; and ⑥ hardening or softening. Finn et al. (1977)[8] took account of these factors in their hyperbolic type nonlinear model.

The modified Ramberg-Osgood models and hyperbolic models mentioned above can be used to describe the degradation of saturated sand under cyclic loading to a certain degree. But all the available models cannot be applied to characterize the following important events: ①the asymptotic movements of MCSL and MPTL associated with the change of effective stress before initial liquefaction; ②large shear strains that occur at nearly zero effective stress state during cyclic undrained loading after initial liquefaction; ③ alternative changes of positive and negative dilatancy during occurrence of cyclic mobility. These three events are related to the development of shear strain from small to large range under cyclic loading. The new constitutive model presented in this paper can take into account all these effects.

1 Modified Ramberg-Osgood model

1.1 Initial skeleton and hysteresis curves for first cycle

Typical nonlinear skeleton and hysteresis curves un-

* **Foundation item**: Supported by Natural Science Foundation of China (59979012)
Received date: 2003- 05- 12

der the condition without change in mean effective stress are schematically illustrated in Fig. 1. The Ramberg-Osgood relation for skeleton curve in the first cycle is defined as follows:

$$\gamma_d = \frac{\tau}{G_{m,0}}\left|1+\alpha\left|\frac{\tau}{G_{m,0}}\right|^{\beta-1}\right|, \qquad (1)$$

in which, γ_d and τ = current shear strain and shear stress respectively; $G_{m,0}$ = initial shear modulus for initial loading starting from time $t = 0$, and it may be determined by geophysical methods, resonant column tests or empirical relations. Several empirical relationships for determining $G_{m,0}$ have been proposed, most of which relate $G_{m,0}$ with initial mean effective stress σ_0', void ratio e, and shear strain γ. Based on tests for round sands and angular crushed quartz sands, Richart (1975)[9] recommended:

$$G_{m,0} = A\frac{(B-e)^2}{1+e}\sqrt{\sigma_0'}, \qquad (2)$$

where A and B = material dependent parameters. Iwasaki and Tatsuoka (1977)[10] also proposed:

$$G_{m,0} = A(\gamma)B(\gamma)\frac{(2.17-e)^2}{1+e}(\sigma_0')^{m(\gamma)}, \qquad (3)$$

where $A(\gamma)$ and $B(\gamma)$ are a function of γ; $B = 1$ for uniform clean sand for a wide range of grain sizes; and $G_{m,0}$ and σ_0' are in kgf/cm^2. Note that $G_{m,0}$ is usually determined at a very small γ level of 10^{-6} order. This small value of γ is denoted as γ_i.

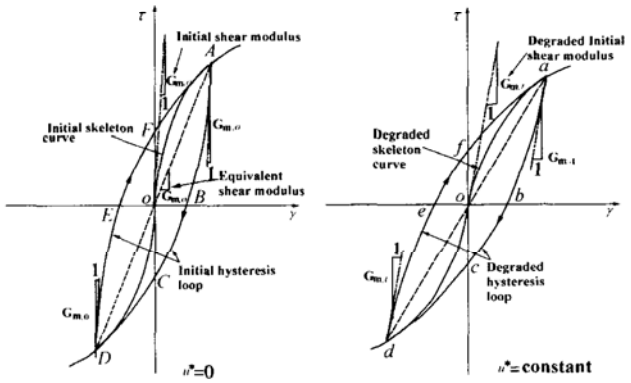

Fig. 1　Schematic illustration of stress strain relation in the first and subsequent cycles under the conditions where the excess pore water pressures u^* are assumed constant within a single cycle

According to Masing criteria, the unloading reloading hysteresis curve can be expressed as

$$\gamma_d \pm \gamma_{rev} = \frac{\tau \pm \tau_{rev}}{G_{m,0}}\left|1+\alpha\left|\frac{\tau \pm \tau_{rev}}{2G_{m,0}}\right|^{\beta-1}\right|, \qquad (4)$$

in which, γ_{rev} and τ_{rev} = shear strain and shear stress at reversal point; α and β in Eq. (4) are estimated by

$$\alpha = \left|\frac{2}{\gamma_{rf,0}}\right|^{\beta-1}, \qquad (5)$$

$$\beta = \frac{2+\pi h_{max}}{2-\pi h_{max}}, \qquad (6)$$

herein, $\gamma_{rf,0}$ = reference shear strain at the value of $G_{eq}/G_{m,0} = 1/2$, where G_{eq} is equivalent shear modulus defined in Fig. 1(a), and h_{max} = maximum damping of soil. Tests show that $\gamma_{rf,0}$ depends on the initial mean effective stress σ_0' and it is readily determined according to experimental $G_{eq}/G_{m,0} - \gamma$ curve.

1.2　Degraded skeleton and hysteresis curves for subsequent cycles

The basic feature of saturated sand under cyclic loading is its tendency to contract. In undrained conditions, the seepage of the pore water is restricted and thus the excess pore water pressure u^* builds up while effective confining stress σ' decreases. In the loading process from the second to subsequent cycles, the initial shear modulus, $G_{m,t}$, tends to decrease due to increase in u^* and thus γ. This leads to degradation of the skeleton curve, as illustrated in Fig. 1(b) which shows the degraded skeleton curve with the degraded initial shear modulus $G_{m,t}$. If u^* is assumed constant within a single cycle, the stress-strain behavior of the second and subsequent cycles can be characterized by the degraded skeleton curve in conjunction with the Masing criteria. In this situation, $G_{m,0}$ in Eq. (1) is replaced by $G_{m,t}$, and the degraded skeleton curve is expressed by

$$\gamma_d = \frac{\tau}{G_{m,t}}\left|1+\alpha\left|\frac{\tau}{G_{m,t}}\right|^{\beta-1}\right|. \qquad (7)$$

1.3　Degradation and hardening of skeleton and hysteresis curves

The actual stress-strain behavior for a specified cycle is shown in Fig. 2. This indicates that u^* is not constant even within a single cycle, showing a significant increase during negative dilatancy and decrease during positive dilatancy. Consequently, the stress strain relation shown in Fig. 2(b) obviously differs from that in Fig. 1(b). Since $G_{m,t}$ is a function of mean effective stress which in turn depends on the contemporaneous rate of the excess pore pressure change, the skeleton curve varies in this single loading cycle. Fig. 3 shows the tendency of degradation of the skeleton curve due to negative dilatancy and then hardening due to positive dilatancy. It means that the modeling of the actual stress-strain behavior can be made by using a changing skeleton curve in conjunction with the Masing criteria. Such a skeleton curve can be expressed as long as $G_{m,t}$ is determined according to current mean effective confining stress σ_t'. At this time, the skeleton curve can be given in terms of the incremental expression of Eq. (7) as

$$d\gamma_d = \frac{d\tau}{G_{m,t}}\left|1+\alpha\beta\left|\frac{\tau}{G_{m,t}}\right|^{\beta-1}\right|, \qquad (8)$$

and accordingly, the hysteresis loop may be written by

$$d\gamma_d = \frac{d\tau}{G_{m,t}}\left|1+\alpha\beta\left|\frac{\Delta\tau}{2G_{m,t}}\right|^{\beta-1}\right|, \qquad (9)$$

in which $\Delta\tau$ = an incremental shear stress from the latest reversal point of cyclic stress, as defined in Fig. 1.

By Eq. (3), $G_{m,t}$ is determined by

$$G_{m,t} = A(\gamma)B(\gamma)\frac{(2.17-e)^2}{1+e}(\sigma_t')^{m(\gamma)}. \quad (10)$$

Thus, the ratio of $G_{m,t}$ to $G_{m,0}$ may be given as

$$\frac{G_{m,t}}{G_{m,0}} = \frac{A(\gamma_t)(\sigma_t')^{m(\gamma_t)}}{A(\gamma_i)(\sigma_i')^{m(\gamma_i)}}, \quad (11)$$

in which γ_i = shear strain of 10^{-6} order at initial state (time $t = 0$), as defined before, and γ_t = shear strain at time t. If $A(\gamma_t)/A(\gamma_i)$ is approximately taken unity and $m(\gamma_i) = m(\gamma_t) = m$ where m = constant, then Eq. (11) becomes

$$G_{m,t} = G_{m,0}\left|\frac{\sigma_t'}{\sigma_0'}\right|^m = G_{m,0}\left|\frac{\sigma_0' - u^*}{\sigma_0'}\right|^m. \quad (12)$$

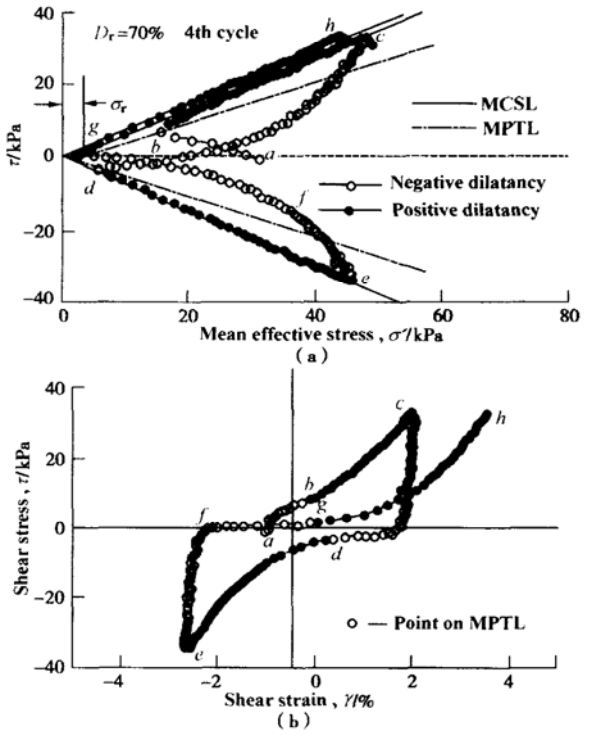

Fig. 2 Stress-strain behavior of saturated sand within a single cycle

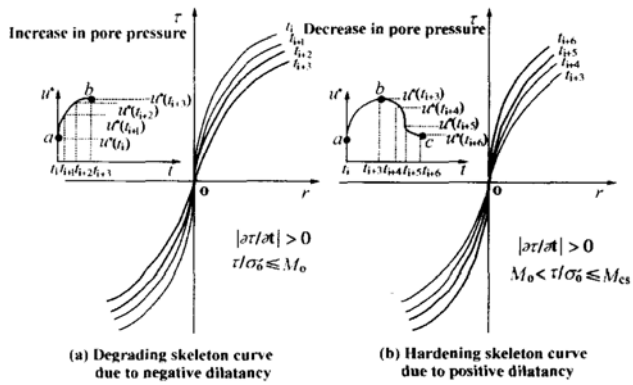

Fig. 3 Schematic illustration of degradation and hardening of skeleton curve due to negative and positive dilatancy

Many investigations showed that a linear-logarithmic relationship with a slope of approximately 0.5 exists between shear modulus and mean effective stress as indicated by Eq. (2). Therefore, $m \approx 0.5$.

In addition, the reference shear strain $\gamma_{rf,t}$ at time t, which is similar to $\gamma_{rf,0}$ as in Eq. (5), depends on the effective confining pressure. It is estimated by the formula (Shamoto & Shimizu, 1986[11]):

$$\gamma_{rf,t} = \gamma_{rf,0}\left|\frac{\sigma_t'}{\sigma_0'}\right|^{m_\gamma} = \gamma_{rf,0}\left|\frac{\sigma_0' - u^*}{\sigma_0'}\right|^{m_\gamma}, \quad (13)$$

in which m_r = a parameter, usually $m_r = m$. Correspondingly,

$$\alpha = \left|\frac{2}{\gamma_{rf,t}}\right|^{\beta-1}, \quad (14)$$

in which, β is the same as that defined in Eq. (6).

2 Asymptotic movements of MCSL and MPTL

As can be known from the above description, the determination of the excess pore water pressure u^* is the key issue formulating the cyclic undrained stress-strain behavior. Fig. 2 shows that the increase or decrease in u^* under cyclic undrained loading is related to the occurrence of negative or positive dilatancy. The negative and positive dilatancy can be separated by MPTL, and in addition, the mobilized maximum shear-normal stress ratio associated with positive dilatancy can be determined by MCSL. (Zhang, 1994[12]; Zhang, et. al., 1997 & 1999[13~15]) The asymptotic movements of the two lines have been illustrated in Fig. 4.

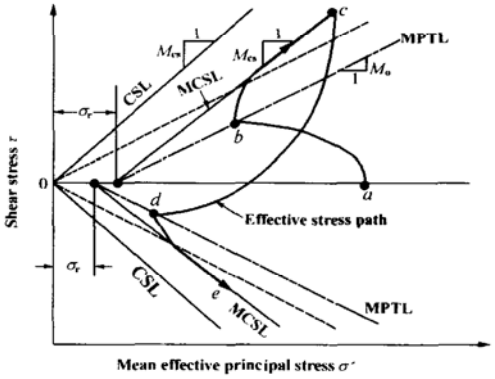

Fig. 4 A formulation for determining change in the effective stress path related with negative and positive dilatancy

Before the effective stress state point attains MPTL for the first time, the rate of generation of u^* is estimated by extending the following empirical equation proposed by Seed et al. (1976)[16]:

$$\frac{u^*}{\sigma_0'} = \frac{2}{\pi}\arcsin(R_N^{1/a_f}), \quad (15)$$

in which a_f = a function of the soil property and loading conditions, and R_N = cyclic ratio defined by a ratio between number of applied stress cycles N and accumulative number of cycles required to cause initial liquefaction N_L. Unlike the laboratory test conditions where a constant amplitude cyclic loading is used in common, the loading conditions in the field during an earthquake are random in nature. In order to fit this requirement, the evaluation of the

parameters in Eq. (15) may be made using the following equations (Shamoto & Shimizu, 1986[11]):

$$R_N = \sum A \left| \frac{1}{N_i} - \frac{1}{N_{i-1}} \right|, \tag{16}$$

$$N_i = 2C_3 \left| \frac{|\Delta\tau|}{2\sigma_0' C_1} \right|^{1/C_2}, \tag{17}$$

$$C_1 = \left| \frac{1}{20} \right|^{C_2} R_{20}, \tag{18}$$

in which $A = 1$, $C_2 = -0.25$, $C_3 = 1$, and R_{20} = shear stress ratio causing initial liquefaction at 20th cycle. Eq. (17) can be derived assuming that the relationship between the cyclic shear stress ratio and the number of cycles causing liquefaction is linear on a log-log plot.

For loading phases once after the effective stress point hits MPTL, the decrease in the excess pore water pressure u^* due to positive dilatancy may approximately be given by

$$\Delta u^* = -\frac{|\sigma(\sigma_0' - \sigma_r') - M_0|}{|M_{cs} - M_0|} \left| \frac{\Delta\tau}{M_{cs}} \right|,$$
$$(M_0 < |\sigma(\sigma_0' - \sigma_r)| < M_{cs} \;\&\; \partial|\tau|/\partial t > 0), \tag{19}$$

and

$$\Delta u^* = -\frac{\Delta\tau}{M_{cs}},$$
$$(|\sigma(\sigma_0' - \sigma_r)| = M_{cs} \;\&\; \partial|\tau|/\partial t > 0). \tag{20}$$

The signs adopted in Eqs. (19) and (20) are demonstrated in Fig. 4. The reference stress may be estimated by following formula:

$$\begin{cases} \dfrac{\sigma_r}{\sigma_0'} = 1 - \dfrac{\dfrac{\Delta\gamma_a}{(\Delta\gamma_a)_{cr}}}{C_4 + C_5 \dfrac{\Delta\gamma_a}{(\Delta\gamma_a)_{cr}}} & \Delta\gamma_a < (\Delta\gamma_a)_{cr}, \\ \dfrac{\sigma_r}{\sigma_0'} = 0 & \Delta\gamma_a < (\Delta\gamma_a)_{cr}, \end{cases} \tag{21}$$

in which σ_0' is initial mean effective principle stress, $\Delta\gamma_a$ is called "accountable shear strain increment", defined as the shear strain increment during loading phase in which negative dilatancy occurs, such as a to b, c to d or e to g in Fig. 2. $(\Delta\gamma_a)_{cr}$ is the critical value of $\Delta\gamma_a$, and $\sigma_r = 0$ when $\Delta\gamma_a \geqslant (\Delta\gamma_a)_{cr}$. C_4 and C_5 are the functions of relative density. The detailed description can be found in Ref. [13~15].

As shown in Fig. 4, after the loading phase associated with positive dilatancy from point b to c, negative dilatancy takes place in the subsequent stress path phase starting from the reversal point c to the next point d on MPTL. The rate of the increase in u^* due to negative dilatancy may be estimated by Eq. (16) with A-value that is greater than 1 and increases with the application of shear stress.

Eqs. (12) ~ (21) provide a stress degradation model for defining the degradation of the shear modulus and the reference shear strain due to reduction in the mean effective confining stress during cyclic undrained loading.

3 A shear strain component independent of effective stress

A great deal of laboratory experiments show that large deformation always occurs after initial liquefaction, and in particular, can develop when the effective confining stress in sand momentarily goes through zero state during undrained loading. For the case of cyclic undrained loading after initial liquefaction as shown in Fig. 5, the effective stress becomes zero twice in one loading cycle. The stress-strain hysteresis curve in a single cycle can be divided into two stress states, i.e., zero and non-zero effective confining stress states. The stress-strain hysteresis curves associated with non-zero effective confining stress states are parallel to each other. This indicates that the changes in shear strain occurring during the non-zero stress states are almost the same. Conversely, the shear strain induced at zero effective confining stress state increases with increasing number of load cycles, but its change doesn't relate with the change in effective stress. Therefore, the latter component of shear strain governs the increase in shear strain after initial liquefaction.

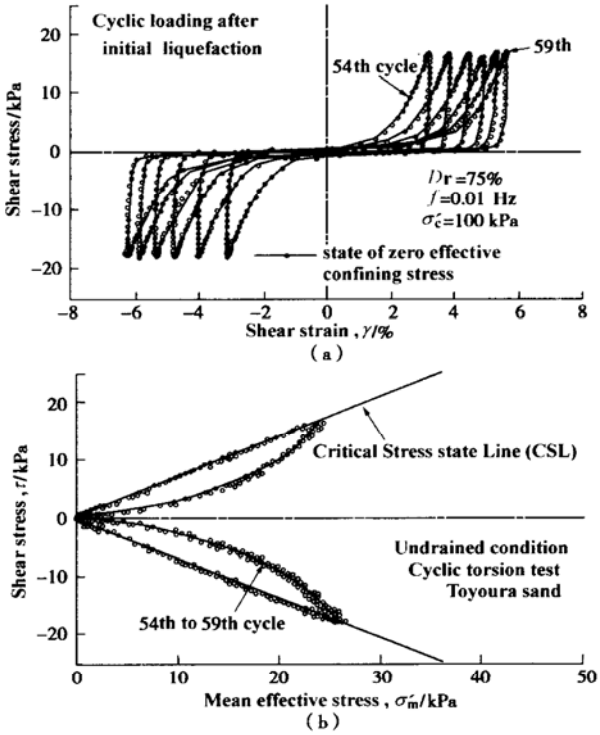

Fig. 5　Two post-liquefaction shear strain components observed in typical cyclic undrained torsional shear tests

Based on such an experimental finding, Shamoto, Zhang & Goto (1997)[17] indicate that two shear strain components exist during post-liquefaction cyclic undrained loading, and thus, a post-liquefaction shear strain γ may be expressed as

$$\gamma = \gamma_d + \gamma_0, \tag{22}$$

in which γ_d = a shear strain component occurring during shearing in non-zero effective confining stress states and γ_0 = a shear strain component occurring during shearing in

zero effective confining stress states. The shear strain component γ_0 plays a decisive role in the development of large post-liquefaction shear strain.

Obviously, γ_d is dependent on the change in effective stress and can be determined using the constitutive model described already in sections 1 and 2. γ_0 is independent on the change in effective stress. Therefore, $\gamma_0 = 0$ and thus $\gamma = \gamma_d$ before initial liquefaction.

On the basis of new physical model of dilatancy, relative compression concept, theory of plasticity and other previous available studies, Shamoto, Zhang and Goto (1997)[17] proposed the following constitutive relation for determining the shear strain component γ_0:

$$\gamma_0 = \frac{R_0}{M_{cs}} \frac{e_0 - e_{min}}{1 + e_0} (\gamma_{max} - \gamma_{entry})^m, \quad (23)$$

$$\gamma_{entry} = \left| - R_0 \frac{e_0 - e_{min}}{1 + e_0} \varepsilon_{vc,0} \right|^{1/m}, \quad (24)$$

in which γ_{max} and γ_{entry} are, respectively, maximum double amplitude shear strain induced by preceding cyclic undrained loading and minimum double amplitude shear strain required to cause initial liquefaction named "entrance shear strain"; e_0 and e_{min}, the current and minimum void ratio; m, and R_0 = material constants determined by tests, and particularly, $m = 0.76$ and $R_0 = 28.1$ for loose to medium dense clean sand; $\varepsilon_{vc,0}$ = the volumetric strain of expansion due to reduction in mean effective confining stress at state of zero effective confining stress, and $\varepsilon_{vc,0} < 0$ because the volume strain takes negative sign for expansion.

4 Performance of the model

A new constitutive model for determining the cyclic undrained stress-strain behavior over a wide range from small to large strains has been established. It is composed of Eqs. (22), (9), (23) and other related equations, in which the determination of the model parameters involved has been described before.

The experimental results obtained from cyclic undrained torsional shear tests for saturated Toyoura sand ($\rho_s = 2.65$ g/cm^3, $D_{50} = 0.18$ mm, $e_{max} = 0.973$ and $e_{min} = 0.635$) are adopted in order to confirm the effectiveness of the proposed model. In testing, all the samples were prepared by pluviating dry sand through air, and were saturated by circulating CO_2 gas, percolating de-aired water and then by applying a back pressure of 100 kPa. B-value of more than 0.96 was obtained for all the samples. The samples were consolidated isotropically under an initial effective consolidation stress σ_c' of 100 kPa. Sinusoidal cyclic loads were applied on the samples at a frequency of 0.1 Hz. For comparison, several samples with $D_r = 75\%$ were subjected to cyclic loading of either constant or irregular amplitude.

If a time history of cyclic stress tested is used as an "input", then time histories of corresponding excess pore pressure and shear strain can be calculated using the proposed model. A comparison in Fig. 6 for a $D_r = 70\%$ specimen is made between predicted and tested results. The corresponding stress paths and stress-strain relations calculated and tested are compared in Fig. 7. A similar comparison is made in Fig. 8 for a specimen with $D_r = 48\%$. Considerably good agreement exists between calculated and tested results, showing the effectiveness of the new model in the characterization of the undrained response of saturated sand to a constant amplitude cyclic loading application.

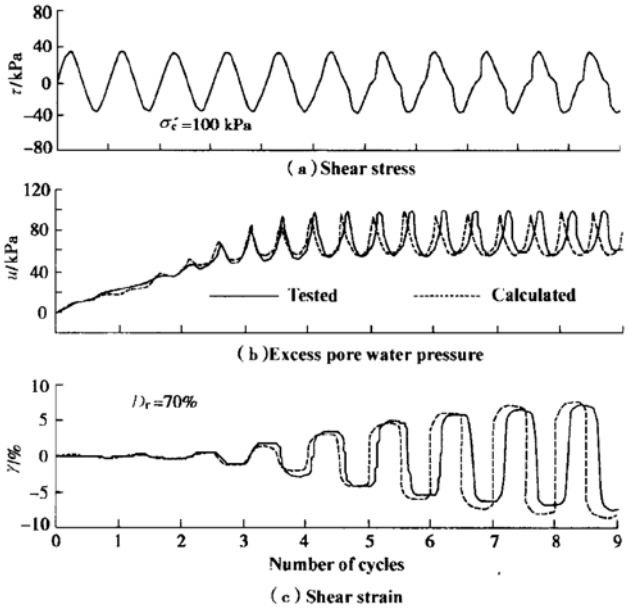

Fig. 6 A comparison between the tested and calculated results for the Toyoura sand with $D_r = 70\%$

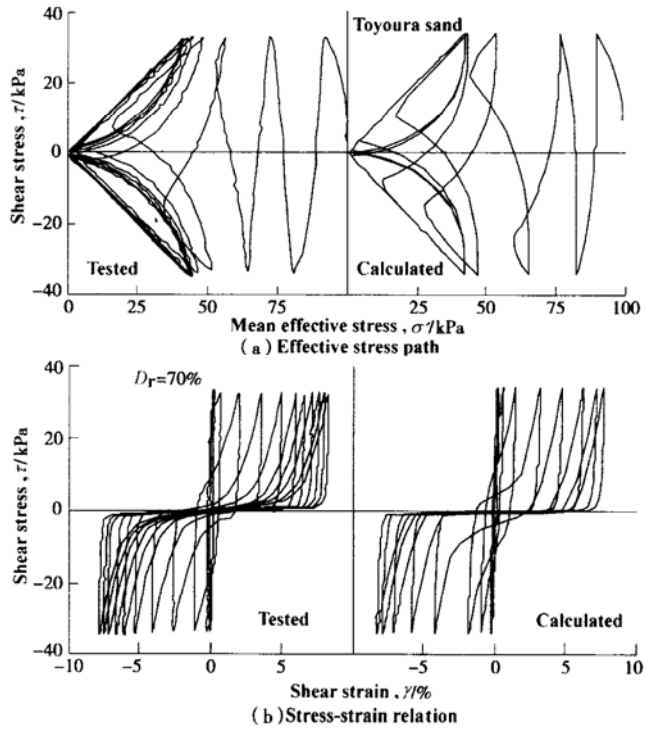

Fig. 7 A comparison between the tested and calculated results for the Toyoura sand with $D_r = 70\%$ (the data used here are the same as those in Fig. 6)

Further calculations were carried out for irregular cyclic loading conditions and the results were plotted in figures 9 and 10. In the same figures, the tested data were also given out. The comparison shows that the calculated results are fairly consistent with the experimental observations. This suggests that the proposed model is a useful tool for accurate cyclic characterization of saturated liquefiable sand in the effective stress analysis of earthquake response.

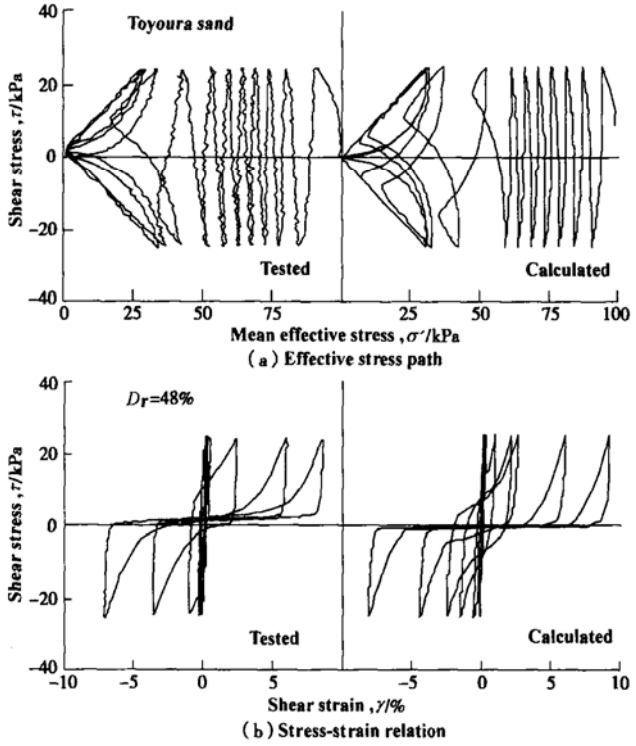

Fig. 8　A comparison between the tested and calculated results for the Toyoura sand with D_r = 48%

5　Summary

The well-known cyclic characterization that employs the concept of Ramberg-Osgood curve in conjunction with the Masing rule has been refined and verified in this paper. The following three aspects of the refinement are encompassed.

(1) The formulation representing the asymptotic movements of both MPTL and MCSL was incorporated into the modified Ramberg-Osgood model in order to describe accurately the effective stress path and the critical stress states.

(2) A stress degradation model was suggested to reproduce the positive and negative dilatancy and define the degradation and hardening of the first and subsequent skeleton curves with the changing excess pore water pressure.

(3) The modified Ramberg-Osgood model is coupled to the formulation of a new post-liquefaction deformation theory for modeling large cyclic undrained stress-strain behavior after initial liquefaction.

The results calculated by the proposed model have been compared with experimental observations. The con-

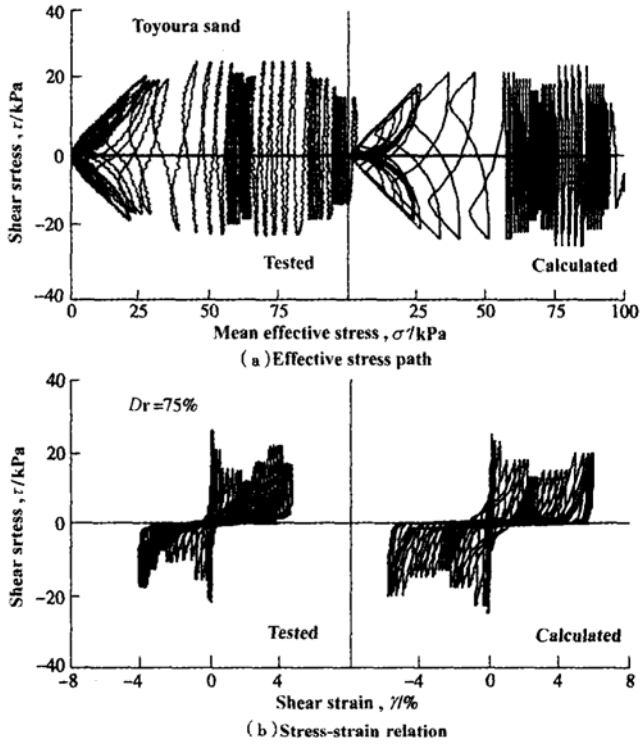

Fig. 9　A comparison between the tested and calculated results for the with Toyoura sand with D_r = 70% subjected to irregular cyclic loading of Pattern 1

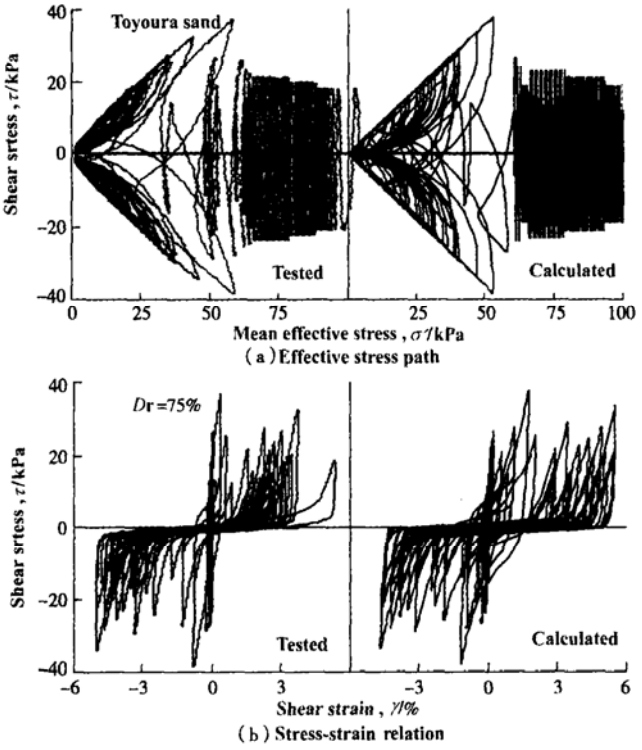

Fig. 10　A comparison between the tested and calculated results for the Toyoura sand with D_r = 70% subjected to irregular cyclic loading of Pattern 2

siderably good agreement between the two suggests that the proposed model is valid for accurate evaluation of cyclic undrained stress-strain behavior of saturated liquefiable sand over a wide range from small to large strains. Although

relatively simple, the presented model provides a new approach for the cyclic characterization of saturated sand, and may be extended for more complicated stress-strain conditions.

References:

[1] Ramberg W, Osgood W R. Description of stress-strain curves by three parameters(NACA Tech Note No 902)[R]. Washington, D C, 1943.

[2] Richart F E. Some effects of dynamic soil properties on soil-structure interaction[J]. Journal of Geotechnical Engineering Division, ACSE, 1975, **101**(12): 1197- 1240.

[3] Idriss I M, Dobry R, Singh R D. Nonlinear behavior of soft clays during cyclic loading[J]. Journal of Geotechnical Engineering Division, ACSE, 1978, **104**(12): 1427- 1447.

[4] Ishihara K. Evaluation of soil properties for use in earthquake response analysis[A]. R Dungar, J A Studer, Eds. Geomechanical Modeling in Engineering Practice[C]. Rotterdam, The Netherlands: A A Balkema, 1986. 241- 275.

[5] Kondner R L, Zelasko J S. A hyperbolic stress-strain formulation of sands[A]. Proceedings, 2nd Pan American Conference on Soil Mechanics and Foundation Engineering[C]. Sao Paulo, Brazil: Brazilian Association of Soil Mechanics, 1963. 289- 324.

[6] Hardin B O, Drnevich V P. Shear modulus and damping in soils: design equations and curves[J]. Journal of Soil Mechanics and Foundation Division, ASCE, 1972, **98**(7): 667- 692.

[7] Prevost J H, Keane C M. Shear stress-strain curve generation from simple material parameter[J]. Journal of Geotechnical Engineering Division, ACSE, 1990, **116**(8): 1255- 1263.

[8] Finn W D L, Lee K W, Martin G R. An effective stress model for liquefaction[J]. Journal of Geotechnical Engineering Division, ACSE, 1977, **103**(6): 517- 533.

[9] Richart F E. Some effects of dynamic soil properties on soil-structure interaction[J]. Journal of Geotechnical Engineering Division, ACSE, 1975, **101**(12): 1197- 1240.

[10] Iwasaki T, Tatsuoka F. Effect of grain size on dynamic shear modulus of sands[J]. Soils and Foundations, 1977, **17**(3): 17- 35.

[11] Shamoto Y, Shimizu K. The applicability of a one-dimensional liquefaction analysis with cyclic mobility to loose and dense sand layer[A]. Proceedings, 7th Japan Earthquake Engineering Symposium[C]. 1986. 685- 690. (in Japanese).

[12] Zhang J M. Transient shear strength of saturated sand under cyclic loading considering strain-rate effect[J]. Soils and Foundations, 1994, **34**(4): 51- 65.

[13] Zhang J M, Shamoto Y, Tokimatsu K. Moving critical and phase-transformation stress state lines of saturated sand during cyclic undrained shear[J]. Soils and Foundations, 1997, **37**(2): 51- 59.

[14] Zhang J M. Cyclic critical stress state theory of sand with its application to geotechnical problems (Technical Research Report RU97007)[R]. Tokyo: Institute of Technology, Shimizu Corporation, 1997. 1- 269.

[15] Zhang J M, Shamoto Y, Tokimatsu K. Cyclic critical stress states of sand with non-frictional effects[J]. Journal of Engineering Mechanics, ASCE, 1999, **125**(10): 1106- 1114.

[16] Seed H B, Martin P P, Lysmer J. Pore water pressure changes during soil liquefaction[J]. Journal of Geotechnical Engineering Division, ASCE, 1976, **102**(4): 323- 346.

[17] Shamoto Y, Zhang J M, Goto S. Mechanism of large post-liquefaction deformation in saturated sands[J]. Soils and Foundations, 1997, **37**(2): 71- 80.